Research Article

A flexible electrode array for determining regions of motor function activated by epidural spinal cord stimulation in rats with spinal cord injury

https://doi.org/10.4103/1673-5374.320987

Date of submission: January 23, 2021

Date of decision: February 25, 2021

Date of acceptance: March 25, 2021

Date of web publication: August 4, 2021

Guang-Wei Mao[1], Jian-Jun Zhang[1], Hao Su[1], Zhi-Jun Zhou[2], Lin-Sen Zhu[2], Xiao-Ying Lü[1, 3, *], Zhi-Gong Wang[2, 3, *]

Graphical Abstract *A high-density flexible array was used to determine the epidural-spinal-cord-stimulated motor function regions (ESCSMFRs) in rat models of complete spinal cord injury (SCI)*

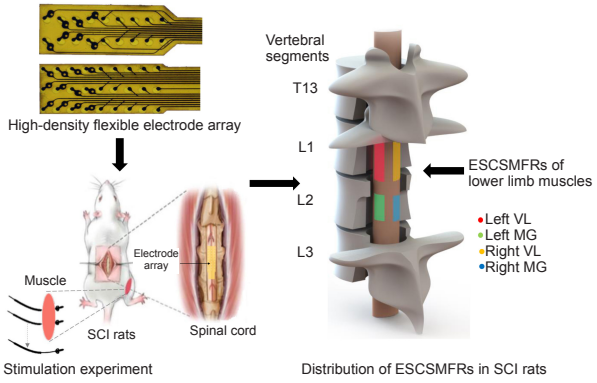

Abstract

Epidural stimulation of the spinal cord is a promising technique for the recovery of motor function after spinal cord injury. The key challenges within the reconstruction of motor function for paralyzed limbs are the precise control of sites and parameters of stimulation. To activate lower-limb muscles precisely by epidural spinal cord stimulation, we proposed a high-density, flexible electrode array. We determined the regions of motor function that were activated upon epidural stimulation of the spinal cord in a rat model with complete spinal cord, which was established by a transection method. For evaluating the effect of stimulation, the evoked potentials were recorded from bilateral lower-limb muscles, including the vastus lateralis, semitendinosus, tibialis anterior, and medial gastrocnemius. To determine the appropriate stimulation sites and parameters of the lower muscles, the stimulation characteristics were studied within the regions in which motor function was activated upon spinal cord stimulation. In the vastus lateralis and medial gastrocnemius, these regions were symmetrically located at the lateral site of L1 and the medial site of L2 vertebrae segment, respectively. The tibialis anterior and semitendinosus only responded to stimulation simultaneously with other muscles. The minimum and maximum stimulation threshold currents of the vastus lateralis were higher than those of the medial gastrocnemius. Our results demonstrate the ability to identify specific stimulation sites of lower muscles using a high-density and flexible array. They also provide a reference for selecting the appropriate conditions for implantable stimulation for animal models of spinal cord injury. This study was approved by the Animal Research Committee of Southeast University, China (approval No. 20190720001) on July 20, 2019.

Key Words: electrode array; epidural spinal cord stimulation; evoked potentials; motor function; rehabilitation; spinal cord injury; spinal segment

Chinese Library Classification No. R459.9; R363; R364

Introduction

Spinal-cord injury (SCI) caused by falling from high altitude, traffic accidents, and disease are common and serious (Jain et al., 2015). In 2016, there were more than 900,000 new cases SCI globally (GBD 2019 Viewpoint Collaborators, 2020). Different degrees of SCI can affect or even completely cut off the functional communication from the brain to the spinal cord below the injured site (Maynard et al., 1997). This leads to functional disorders of the motor, sensory, and autonomic nerves below the level of injury, including symptoms, such as dyspnea, limb paralysis, and urethral dysfunction. Spinal-cord neurons cannot regenerate (Wang et al., 2013). Thus, the impact of SCI is lifelong and bring heavy burden to patient, family, and society. The treatment of SCI remains a major unmet need in medical science (World Health Organization, 2013; Griffin and Bradke, 2020).

Common treatment methods to recover the motor function of lower limbs of persons with SCI include biomedical approaches

[1]State Key Laboratory of Bioelectronics, Southeast University, Nanjing, Jiangsu Province, China; [2]Institute of RF- & OE-ICs, Southeast University, Nanjing, Jiangsu Province, China; [3]Co-innovation Center of Neuroregeneration, Nantong University, Nantong, Jiangsu Province, China

***Correspondence to:** Xiao-Ying Lü, PhD, luxy@seu.edu.cn; Zhi-Gong Wang, PhD, zgwang@seu.edu.cn.

https://orcid.org/0000-0002-3777-2472 (Xiao-Ying Lü); https://orcid.org/0000-0002-9203-4683 (Zhi-Gong Wang)

Funding: *This work was supported by the National Natural Science Foundation of China, Nos. 61534003 (to ZGW) and 61874024 (to ZGW).*

How to cite this article: *Mao GW, Zhang JJ, Su H, Zhou ZJ, Zhu LS, Lü XY, Wang ZG (2022) A flexible electrode array for determining regions of motor function activated by epidural spinal cord stimulation in rats with spinal cord injury. Neural Regen Res 17(3):601-607.*

(Fischer et al., 2020; Xu et al., 2020; Zheng et al., 2020), physical rehabilitation (Young and Ferris, 2017), transcutaneous stimulation (Luo et al., 2020), and spinal-cord stimulation (Ichiyama et al., 2005; Harkema et al., 2011; Angeli et al., 2018; Dalrymple et al., 2018; Gill et al., 2018; Wagner et al., 2018). The modalities of spinal-cord stimulation include intraspinal microstimulation and epidural spinal-cord stimulation (ESCS) (Grahn et al., 2014). ESCS places stimulating electrodes on the surface of the spinal dura to activate the spinal-cord neural network. ESCS was first proposed in 1967 by Sheary et al. to relieve the pain of cancer patients. It has since been used to achieve clinical effects on analgesia, urination, and motor function recovery (Khanna, 2016). In contrast with intraspinal microstimulation, ESCS is non-invasive to the spinal cord (Khanna, 2016), giving it greater clinical utility. Recent clinical reports (Angeli et al., 2018; Gill et al., 2018; Wagner et al., 2018; Gorgey et al., 2020) showed that, with the combination of ESCS and long-term rehabilitation training, motor functions were recovered in persons with SCI, such as standing and walking with the help of rehabilitation devices. Theoretical (Struijk et al., 1993; Rahal et al., 2000; Holsheimer, 2002) and experimental studies (Minassian et al., 2004; Lavrov et al., 2008) on the use of ESCS for the recovery of limb motor functions showed that the stimulation may directly activate the posterior root fibers of the spinal cord, thereby activating the spinal motor network and restoring muscular movement of lower-limb muscles.

Our research group proposed a novel method to reconstruct motor functions using a micro-electronic neural bridge (MENB) (Wang et al., 2008, 2009; Shen et al., 2013; Huang et al., 2016). A MENB consists of a micro-electronic module with two micro-electrode arrays, the first for neural signal detection and the second for functional electrical stimulation of nerves. The module amplifies the spontaneous neural signals detected by the first micro-electrode array from the spinal cord above the injured site. It then processes and regenerates the amplified signals for electrical stimulation using a sorting algorithm. The regenerated signals are used to stimulate spinal cord below the injured site, so that the neural function of the injured spinal cord can be rebuilt. Thus, an MENB system acts as a multiple point-to-point relay and as neural-function rebuilder. Because ESCS can be more easily promoted in clinical practice than intraspinal microstimulation (Harkema et al., 2011), we chose ESCS as the stimulation mode for MENB.

The recovery time for persons with SCI is varied and determined by the ESCS strategy (Formento et al., 2018). Although most ESCS strategies have constant stimulation sites and parameters (Harkema et al., 2011; Angeli et al., 2018; Gill et al., 2018), spatiotemporal neuro-modulation of ESCS (Wagner et al., 2018) can lead to be greater recovery of movement, and reduced rehabilitation duration. This has demonstrated that the position, parameters, and sequence of ESCS are crucial to recovery (Lavrov et al., 2008). Therefore, to optimize the ESCS technique, it is necessary to study the relationship between the stimulation site, stimulation parameters, and the motion responses to stimulation.

At present, the ESCS electrodes used in clinical trials are mainly designed to treat analgesia (Harkema et al., 2011; Wong et al., 2017; Gill et al., 2018). For the recovery of movement, a higher spatial resolution is needed than for treating analgesia. Some studies have designed ESCS electrode arrays for animal modes (Zhou et al., 2012; Gad et al., 2013; Xu et al., 2015; Wenger et al., 2016; Wang et al., 2021), but these electrodes do not provide sufficiently high spatial resolution for animal models and humans. Gad et al. (2013) showed that increasing the number of electrodes can improve control of the stimulation responses and the stimulation site. Their high-density flexible electrode array improved the spatial resolution of experimental and commercial epidural stimulation electrodes, thereby enhancing the selective activation of lower limb muscles in a rat model of complete SCI.

In this paper, we present a high-density flexible electrode array that can determine the regions of motor function of the lower-limb muscles that respond to spinal-cord stimulation (we refer to these regions as 'epidural-spinal-cord-stimulated motor function regions' or ESCSMFRs). Furthermore, the relationship between the stimulation site and parameters of different spinal segments and the motion response of lower-limb muscles was studied. By identifying the optimal stimulation parameters, our findings will serve to improve the accuracy of activation of lower-limb muscles.

Materials and Methods

Animals

A total of eight specific-pathogen-free female Sprague-Dawley rats weighing 180–200 g and aged 7–8 weeks were provided by Zhejiang Experimental Animal Center, China (license No. SCXK (Zhe) 2019-0002). All experimental processes mentioned below comply with Guidelines for the Care and Use of Laboratory Animals of the US National Institutes of Health (No. 85-23, revised 1996), and all surgical operations were performed under sterile conditions. All rats were housed in a clean incubator under controlled conditions of 25°C and a 12-hour light-dark cycle. This study was approved by the Animal Research Committee of Southeast University, China (approval No. 20190720001) on July 20, 2019.

Preparation of the SCI animal model

The rats were anesthetized with isoflurane gas in oxygen-enriched air (1.5%) (RWD, Shenzhen, Guangdong Province, China), followed by a partial laminectomy performed at the T8 vertebrae to expose the spinal cord. A section of spinal cord (approximately 2 mm) was taken out with ophthalmic scissors. Afterwards, fine-pointed forceps were used to clear the residual tissue along the spinal canal wall, and the incision was plugged with a hemostatic sponge. All wounds were washed by injecting a sodium chloride solution (Hualu, Liaocheng, Shandong Province, China) and then sutured in layers. During the operation, a constant temperature of 37.5°C was maintained using a heating pad (Xinong, Beijing, China).

After the operation, the rats were given food and water three times a day in individual incubators. In the first 3 days after the operation, the rats were treated with 10-mg oral amoxicillin per day (Macklin, Shanghai, China) to prevent infection. The bladders of SCI rats were massaged and the urethral orifice was cleaned three times a day for 4 weeks. To maintain the mobility of the joint, a full range of exercises was also performed with human assistance for the hind limbs of the rats once a day (Roy et al., 1992).

Design and implementation of epidural-stimulation electrodes

The size of the spinal cord of the rats was measured for electrode design after the operation. The designed length and width of two high-density flexible electrode arrays (**Figures 1** and **2**) were 5.8 × 2.2 mm^2. The electrode arrays shown in **Figure 1A** and **1B** were 9 × 3 and 9 × 2, respectively. Because of the limitation of the electrode technology, we could not realize 9 × 5 array in this area. The 9 × 2 array can fill the unused space in the 9 × 3 array.

As shown in **Figure 2**, each electrode was round with a diameter of 0.2 mm, and the horizontal and vertical distance between the centers of adjacent electrodes were 0.9 and 0.6 mm, respectively. **Figure 1C** and **1D** show extended maps of two arrays, including the electrode wiring and positions of the electrodes. **Figure 2A** and **2B** show scanning electron microscope images of two electrode arrays; the gold-plated distribution of the electrodes is demonstrated by energy-dispersive spectroscopy analysis. **Figure 2C** presents the scanning electron microscope image of a single electrode; the associated the energy-dispersive spectroscopy image is

shown in **Figure 2D**.

The substrate of the electrodes was a polyimide film with an upper and lower thickness of 28 μm. Internal wiring was formed through semiconductor processes by a development and etching process. Then, the whole electrode wiring was covered by hot pressing. The thickness of the electrode wiring was 35 μm; the wiring width and distance were 50 μm; and the overall thickness of the electrode was 55 μm. Finally, the shape of electrode was cut with a laser.

Stimulation procedures

Because of spinal shock (Ko et al., 1999), the stimulation experiments were performed 4 weeks after the operation. First, a skin incision at T12–L3 vertebrae of the rat model with SCI was opened to remove the spinous process of the vertebrae, and then the space between the vertebrae was opened to insert the epidural electrode array. The front of the vertebrae was used as the reference point of the electrode position, which was observed with an optical microscope (WPI, Sarasota, Florida, USA). It was easier to use the vertebrae level as the reference point than the level of the spinal cord, which avoided unnecessary injury. We conducted high-density stimulations for the combination of two arrays with segmental movement. The position for effective stimulation corresponding of the spinal cord segment was recorded. After operation, the spinal-cord segments of rats were determined upon removing their vertebrae.

Charge-balanced biphasic current stimulation signals were generated by a Master 9 multi-channel programmable stimulator (AMPI, Jerusalem, Israel) and two ISO-Flex stimulus isolation units (AMPI). The current amplitude of the negative pulse was five times greater than the amplitude of the positive pulse. Because the threshold of SCS at the cathode was lower than that at the anode (Holsheimer et al., 2002; Lavrov et al., 2008), the stimulation effect was mainly the effect of the negative pulse within the first phase. The smaller current of the positive pulse was unable to activate the nerves, and did not interfere with the experimental results. To keep the charge balance and protect the nerves, the width of the negative pulse (200 μs) was one fifth of that of the positive pulse. As shown in **Figure 3**, the cathode was moved sequentially to all electrode sites in the two arrays, and the anode was placed subcutaneously on the side of the rats. Because the threshold of the response to single-synaptic stimulation during repeated stimulation, the interval between stimulating pulses was at least 2 seconds. The stimulation signal was recorded using a 16-channel data acquisition system (AD Instruments, Bellavista, New South Wales, Australia).

Recording of the EMG signals

EMG signals were collected during the stimulation experiments. An incision was opened on the skin of the lower-limb muscles to expose the vastus lateralis (VL), semitendinosus, tibialis anterior, and medial gastrocnemius (MG) muscle. As shown in **Figure 3**, stainless-steel wire electrodes (KD-MW-316, Suzhou, Jiangsu Province, China) were inserted into the muscles by a needle. Then, the tails of the stainless-steel wires were knotted to fix their position. The 10-mm coating in front of the knot in the muscles was exposed to record the electromyographic (EMG) signal. The coating on the heads of the wire electrodes was removed to connect them with a multi-channel physiological signal amplifier (A-M systems, USA) to record the EMG signals of the muscles. The gain was set to 1000 to amplify the EMG signals and the passband of EMG filtering was 10–1000 Hz. The EMG signals were sampled at 40 kHz, and saved, processed, and displayed in real time using a 16-channel Power Lab data-acquisition system (AD Instruments). Electrical stimulation was used to verify the positions of the electrodes in each muscle.

Determination of the ESCSMFRs

The vertebral segments T12–L3 were mapped with two high-density flexible electrode arrays, which were placed on the surface of the dura mater. Initially, a charge-balanced biphasic pulse with a negative phase amplitude of 300 μA and a frequency of 0.2 Hz was applied. The responses of the muscles to stimulation were evaluated from the EMG signals.

The stimulation current was increased or decreased with a step size of 10 μA from 300 μA to determine the responses of specific muscles. When the target muscle began to respond, no response of the other muscles was detected, and the responses of the antagonistic muscle of the target muscle appeared at currents of at least 30 μA. We defined the positions of such stimulation as the ESCSMFRs of the target muscle and recorded the center coordinates (X, Y) of the stimulation site.

We normalized the data to reduce the effect of differences in the spinal cord of rats and to precisely locate the ESCSMFRs. Specifically, the upper transverse diameter, D, and length, L, of the vertebral segment from T12 to L3 were measured. The center coordinates (X, Y) of the stimulation site were normalized by D and L of the vertebral segment being stimulated (Tao et al., 2019). After normalization, the distribution maps of the ESCSMFRs in each rat were drawn in the same coordinate system. The difference in the transverse diameter of the spinal cord in the upper or lower segments of the spinal cord was ignored. From the results of eight rats, a distribution map of ESCSMFRs was drawn.

Differences among ESCSMFRs

To precisely locate the stimulation sites, we investigated the differences between the responses at different stimulation sites in the ESCSMFRs of the VL and MG. We used single stimulation pulses with amplitudes of either 380 and 330 μA (median of the maximum and minimum stimulation current thresholds) to separately stimulate the ESCSMFRs of the VL and MG with the two electrode arrays. The root mean square (RMS) of the stimulation responses in each stimulation site was calculated, as shown in Equation (1):

$$\mathrm{RMS}_{\mathrm{EMG}} = \sqrt{\frac{\sum_{i=1}^{N} x_i^2}{N}} \qquad \text{Equation (1)}$$

through the motor-evoked potentials within 10 ms after its first deflection (Wenger et al., 2016), where N is the number of recording points and x_i is a sampling value of the motor-evoked potentials. Ten stimulation responses were recorded for each electrode within the two electrode arrays in the ESCSMFRs. The average RMS of 10 stimulation responses with these electrode sites was calculated after normalization. Finally, the data were processed with a cubic spline interpolation, and the RMS heat maps of ESCSMFRs were drawn.

Effect of stimulation frequency

The relationship between the stimulation frequency and response was explored to optimize the stimulation parameters. The electrode sites with the strongest average stimulation responses in the ESCSMFRs of the VL and MG were selected. These sites were stimulated with an amplitude of either 330 or 380 μA, and at frequencies of 10–100 Hz. With the step size of 10 Hz, 20 stimulation responses of eight rats at each stimulation frequency were recorded to calculate the average peak-to-peak value. The peak-to-peak values (Hofstoetter et al., 2015) instead of the RMS of the stimulation responses were used as the assessment indicator to avoid errors in the stimulation time.

Data analysis

The motor-evoked potentials and stimulating signals were recorded using a 16-channel data-acquisition system (AD Instruments), which transmitted data with a sampling rate of

40 kHz to LabChart software (AD Instruments) on a personal computer for real-time monitoring, processing, and storage. The RMS and peak-to-peak values of the motor-evoked potentials were used to evaluate the effect of ESCS. These values were calculated with an algorithm written in Matlab 2017 (MathWorks, Natick, MA, USA).

Data were expressed as the mean ± standard deviation. The data were analyzed using SPSS 24.0 software (IBM, Armonk, NY, USA). The normal distribution and variance's homogeneity of data was tested. The data followed a normal distribution and the variance between groups was homogeneous. The significance in the stimulation responses and current of the ESCSMFRs was analyzed using a paired Student's *t*-test and a one-way analysis of variance. Tukey's *post hoc* test was performed when multiple comparisons were needed after one-way analysis of variance. A value of $P < 0.05$ was considered statistically significant.

Results

ESCSMFRs in the different lower-limb muscles

Figure 4 is the ESCSMFR map drawn from the experimental results of eight SCI rats. The lengths and widths of the vertebral and spinal-cord segments were averaged for the eight rats. In the map, the electrode is round for the sake of clarity. As shown in **Figure 4**, the ESCSMFRs of the VL were in the L1 vertebral level, whereas the ESCSMFRs of the MG were in the L2 vertebral level. This means that the L1 and L2 vertebral segments were the optimal stimulation regions for VL and MG, respectively.

Within the ESCSMFRs of the VL and MG, the semitendinosus and TA were simultaneously stimulated when the current was increased to 400 μA. However, no obvious ESCSMFRs of the semitendinosus or TA were found in the experiment. Activation of the waist and hip muscles was found in the T12 and T13 vertebral segments, and the spinal cord of the L3 vertebrae level was associated with the activation of the tail and toe muscles. In addition, ESCS applied in the region between the bilateral ESCSMFRs of the TA or MG irregularly stimulated the leg muscles.

Differences of the response among ESCSMFRs

As illustrated in **Figure 5**, even in one ESCSMFR, the stimulation responses differed among different stimulation sites for a given current. The RMS of the yellow areas was higher (meaning the response to stimulation was stronger) than that of the blue areas. In the ESCSMFRs of the VL, the stimulation responses at the different sites were significantly different ($P < 0.001$). The stimulation responses in the lateral sites of the spinal cord were much stronger than those in the medial sites. By contrast, there was little difference among sites in the MG, with the stimulation responses in the medial sites of the spinal cord being slightly stronger than those in the lateral sites. In **Figure 5**, the highlighted sites in the heat map are those with the strongest stimulation response in the ESCSMFRs. These sites required the smallest stimulation current for a given response and the least unnecessary activation of spinal neuronal circuits. Therefore, stimulation in the highlighted areas was able to accurately control lower-limb movement.

Effects of the stimulation current on the response

To determine the appropriate stimulation current, we studied the relationship between the current and response. We selected the sites that had the largest average stimulation response after normalization in the bilateral ESCSMFRs of the VL and MG. At the selected sites, the average maximum and minimum stimulating currents of the SCI rats are shown in **Figure 6**. The threshold of the ESCSMFRs of the VL (310–400 μA) was larger thanthat in the MG (280–350 μA). The difference in the currents required to activate lower-limb muscles should be considered for the stimulation of fine movement.

We presented the relationship between the stimulation current and the muscle responses as the RMS of the stimulation response, as described by Equation (1). The average and variance of the 10 stimulation responses at the selected sites in the eight SCI rats are shown in **Figure 7**. The responses of the muscles to stimulation increased with increasing current. When the current exceeded the maximum threshold, the rate of increase of the response with current substantially decreased, and other muscles (in particular, antagonist muscles) began to respond, which is an undesirable side effect. Thus, there are maximum and minimum current thresholds for effective stimulation.

Effect of stimulation frequency

As shown in **Figure 8**, the peak-to-peak intensity of the response increased with increasing stimulation frequency. Hence, the intensity of the response was enhanced by ESCS. The rate of change in the intensity decreased with increasing frequency. When the frequency was lower than 25 Hz, the lower-limb muscles of the rats experienced unfused tetanus; at frequencies above 25 Hz, tonic contraction occurred.

The response of the left VL to stimulation in the rat model is shown in **Figure 9**. These results correspond with those of **Figure 8A**. Specifically, a higher stimulation frequency resulted in a shorter response interval. Moreover, the peak-to-peak intensity of the stimulation response for a constant current increased from 4 to 7 Hz as the frequency was increased from 20 to 80 Hz.

Discussion

We investigated the selectivity of the regions of motor function activated by epidural spinal-cord stimulation (ESCSMFRs) in rats using high-density electrode arrays. This technique is already widely used to explore the functional positioning of the nerve-fiber tract, cerebral cortex, and deep-brain structures in animals and humans (Britten and Wezel, 1998; Thier and Andersen, 1998). Although the use of tracers or anatomical methods to dissect nerves can locate the position of motor neurons in the spinal cord (Nicolopoulos-Stournaras and Iles, 1983; Rivero-Melián, 1996), these methods do not capture the responses to stimulation under different parameters. In addition to determining the ESCSMFRs of SCI rats, we determined the characteristics of movement of their lower-limb muscles by ESCS using high-density electrode arrays.

There is currently no specialized stimulating electrode for the recovery of motor function in clinical practice. Therefore, it is imperative to develop a high-density electrode to realize the clinical potential of ESCS. In this study, we developed a high-density flexible electrode array to compensate for the lack of specificity and spatial resolution of ESCS. Our proposed electrode array had a higher spatial resolution than commercially available electrode arrays (Wong et al., 2017) and experimental electrode arrays (Zhou et al., 2012; Gad et al., 2013; Xu et al., 2015; Wenger et al., 2016; Wang et al., 2021). The diameter of the electrode contact used in this experiment was 0.2 mm. This limits the effective range of stimulation to a small area, such that it only affects the nervous tissue in the spinal cord near the site of stimulation. Our results showed that the bilateral VL and MG in rats with complete SCI can be selectively activated using our electrode arrays. By combining two high-density flexible electrode arrays as we have done in this study, ESCS could be used in the future to screen for the optimal stimulation sites for individuals with SCI and to control the muscle force output to accurately activate the movement of the lower limbs.

The ESCSMFR was represented as the region in the spinal cord from which ESCS can selectively activate individual muscles or muscle groups. Through analysis of the movement characteristics of ESCSMFRs, this study provides guidance for both animal experiments and clinical application. The ESCSMFRs of the VL and MG represented the activation pools of the quadriceps and gastrocnemius, respectively, which are key to flexion and extension of the lower limbs. From **Figure 5**, we find that the suitable stimulation sites for the VL and MG are in the lateral area of the L1 and the medial site of the L2 vertebrae segment, respectively. Our work suggests that ESCS primarily activates the spinal afferent nerve and engages proprioceptive feedback circuits. Therefore, the difference between the ESCSMFRs of the VL and MG may be due to the distribution of afferent neurons in the spinal cord. We did not locate the ESCSMFRs of the TA and semitendinosus. The TA and semitendinosus were activated between the ESCSMFRs of the VL and MG, and simultaneously with other muscles.

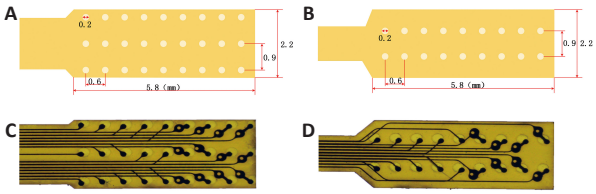

Figure 1 | Diagrams and maps of the stimulating electrode.
(A) Diagram of the 9 × 3 electrode array. (B) Diagram of the 9 × 2 electrode array. (C) Map of the 9 × 3 electrode array. (D) Map of the 9 × 2 electrode array.

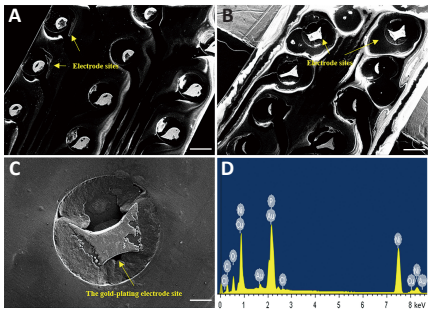

Figure 2 | Scanning electron microscopy analysis of the electrode.
(A) SEM image of the 9 × 3 electrode array. (B) SEM image of the 9 × 2 electrode array. (C) SEM image of a single electrode in the array. (D) Energy-dispersive X-ray spectrum for a single electrode. The yellow arrows indicate the sites of the electrodes in the array. Scale bars in A–C: 100 μm. The impedance of the electrode ranged from 39 to 172 kΩ (0.1 V, 1000 Hz). SEM: Scanning electron microscope.

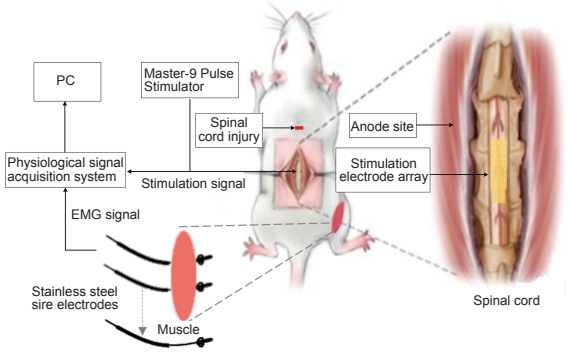

Figure 3 | Schematic diagram of the experimental process.
The experiment was performed 4 weeks after the operation to determine the regions in which motor function was activated upon epidural stimulation of the spinal cord with the combination of two electrode arrays. In the level of the T12–L2 vertebrae segment, the cathode was moved sequentially among all electrode sites of the two arrays, and the anode was placed subcutaneously on the side of the rats. The EMG and stimulation signals were collected for evaluation. EMG: Electromyography.

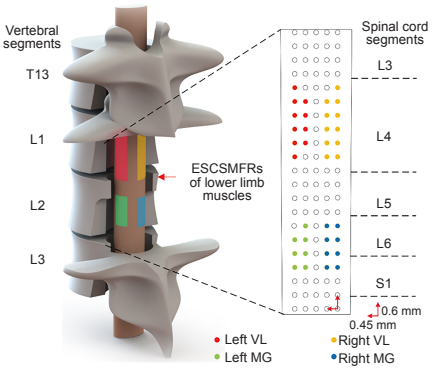

Figure 4 | Regions of the muscles activated upon epidural stimulation of the spinal cord.
The left side of the figure represents the levels of the vertebral segments, and the right side represents the levels of the spinal-cord segments. The sites of electrodes in ESCSMFRs were normalized with the experiment outcome of the eight rats. The red arrows indicate the ESCSMFRs of the lower-limb muscles. The red, yellow, green, and blue regions represent the ESCSMFRs of the left VL, right VL, left MG, and right MG, respectively. ESCSMFR: Epidural-spinal-cord-stimulated motor function region; MG: medial gastrocnemius; VL: vastus lateralis.

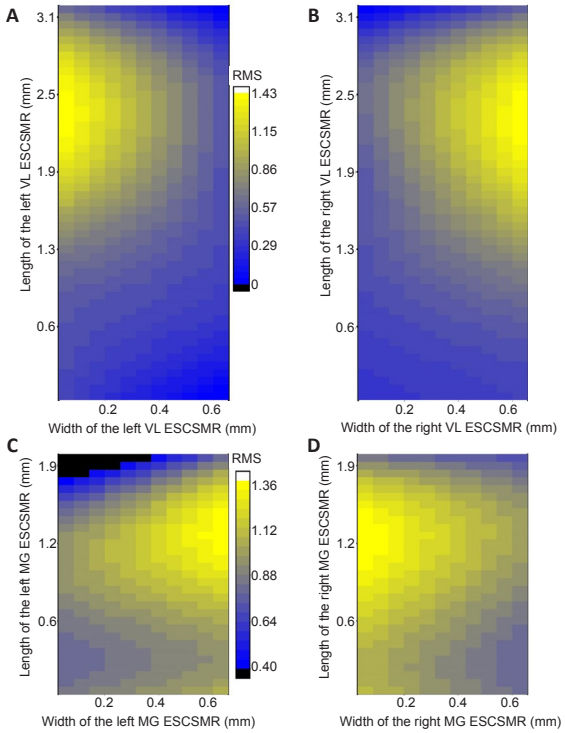

Figure 5 | Stimulation-response heat maps in the regions activated by spinal-cord stimulation.
(A) Heat map of the RMS of stimulation responses of the left VL ESCSMFR; (B) RMS map of the right VL ESCSMFR; (C) RMS map of the left MG ESCSMFR; (D) RMS map of the left MG ESCSMFR. The stimulation currents of the VL and MG were 330 and 380 μA, respectively. The mean RMS value of the stimulation response was averaged for eight rats. The stimulation response was higher in the yellow areas than the blue areas. ESCSMFR: Epidural-spinal-cord-stimulated motor function region; MG: medial gastrocnemius; RMS: root mean square; VL: vastus lateralis.

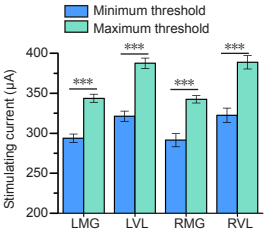

Figure 6 | Maximum and minimum current thresholds in the vastus lateralis and medial gastrocnemius.
The data are shown as the mean ± standard deviation (n = 8). There was a significant difference between the maximum and minimum thresholds of the VL and MG (Student's t-test; ***P < 0.001). LMG: Left medial gastrocnemius; LVL: left vastus lateralis; RMG: right medial gastrocnemius; RVL: right vastus lateralis.

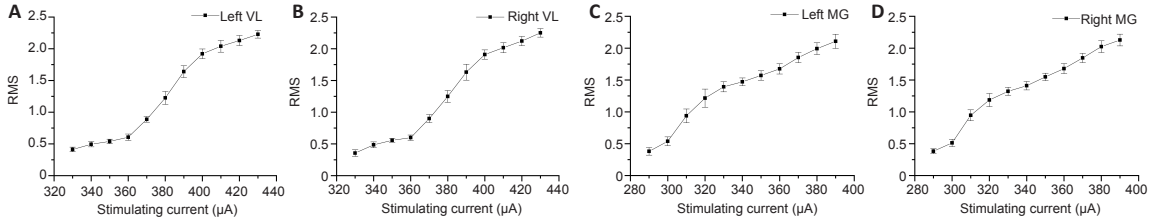

Figure 7 | **Stimulation responses as a function of stimulating current.**
(A) RMS of the stimulation responses in the left VL; (B) RMS of the stimulation responses in the right VL; (C) RMS of the stimulation responses in the left MG; (D) RMS of the stimulation responses in the left MG. The data are expressed as the mean ± standard deviation (*n* = 8; one-way analysis of variance followed by Tukey's *post hoc* test). MG: Medial gastrocnemius; RMS: root mean square; VL: vastus lateralis.

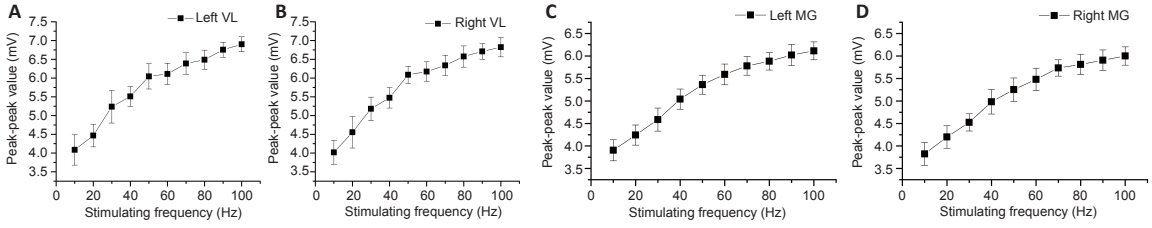

Figure 8 | **Stimulation response as a function of frequency.**
(A) Peak-to-peak values of the stimulation responses in the left VL; (B) peak-to-peak values of the stimulation responses in the right MG; (C) peak-to-peak values of the stimulation responses in the left MG; and (D) peak-to-peak values of the stimulation responses in the right MG. The currents for the VL and MG were 380 and 330 μA, respectively. The peak-to-peak values of eight rats with complete spinal cord injury were recorded at stimulation frequencies of 10–100 Hz. The data are expressed as the mean ± standard deviation (*n* = 8; one-way analysis of variance followed by Tukey's *post hoc* test). MG: Medial gastrocnemius; VL: vastus lateralis.

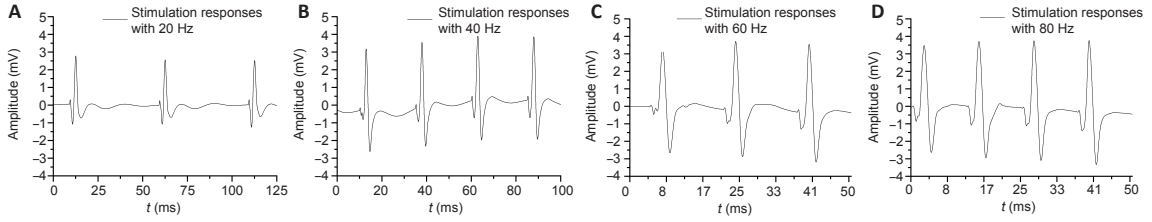

Figure 9 | **Stimulation response of the left vastus lateralis of rats with spinal cord injury for different frequencies at a current of 380 μA.**
(A) 20 Hz; (B) 40 Hz; (C) 60 Hz; (D) 80 Hz.

For a given stimulation frequency, increasing the ESCS current would activate more efferent fibers in the spinal cord (Nelson and Mendell, 1978) and enhance the stimulation response. An excessive current not only triggered a response of the antagonistic muscles, but also other unrelated muscles, which was unfavorable to selective stimulation. There was a difference in the stimulating currents and responses between the ESCSMFRs of the VL and MG. The maximum and minimum threshold currents of the VL were higher than those of the MG. This meant that different muscles required different stimulating currents. The threshold currents of the ESCSMFRs determined in this study are important design parameters.

Increasing the stimulation frequency would raise the firing rate of motor neurons to enhance the response (Gorgey et al., 2006, 2009; Hofstoetter et al., 2015). In this study, with increasing stimulation frequency, the peak-to-peak value of the muscle responses increased. This indicates that a smaller current can be applied by increasing the stimulation frequency, thereby avoiding the activation of undesired muscles. A large stimulating current can block proprioception information and affect the function of the stimulation current (Formento et al., 2018).

ESCS with different frequencies can activate different neural circuits in the spinal cord. For example, stimulation at 50–100 Hz strongly activates the spinal interneurons and inhibits the primary afferent presynaptic nerve of lower limbs (Murg et al., 2000). However, in clinical practice, a stimulation frequency of 25–60 Hz is more commonly used (Minassian et al., 2004; Harkema et al., 2011; Angeli et al., 2018). By optimizing the stimulation parameters (i.e. the frequency and intensity), unnecessary lower-limb movements can be avoided by activating the fewest spinal nerve circuits.

We achieved a high stimulation density by combining two arrays. Our results can be used to design stimulation electrode arrays and stimulation parameters for implantable ESCS and MENB experiments. Future studies need to realize higher-density electrode arrays with more electrodes with smaller diameters within the one electrode slice. This will afford more precise stimulation with finer control of motor function.

Several limitations should be noted regarding this study. First, a high density of electrodes in a single electrode slice was not realized because of limitations of our electrode technology. Second, because the experiment was conducted in anesthetized rats, we could not detect the change of the stimulation responses in SCI rats over time.

In conclusion, our high-density electrode array precisely activated lower-limb muscles, and allowed us to determine the motor-function regions activated by ESCS in the VL and MG. Our results demonstrate the potential of high-density flexible electrode arrays in developing effective treatment methods for SCI.

Acknowledgments: *The authors express their thanks for the guidance about animal experiments from Professor Xiaoyan Shen and Professor Guangming Lü, Nantong University, China and Dr. Bin Zhang, Beijing Tiantan Hospital, China.*
Author contributions: *Design, literature search, experimental studies, statistical analysis, manuscript preparation, manuscript editing: GWM; experimental studies, manuscript editing, data acquisition: JJZ, ZJZ; experimental studies, data analysis: HS; experimental studies, data acquisition: LSZ; concepts, design, definition of intellectual content, manuscript editing, manuscript review, guarantor: ZGW, XYL. All authors*

approved the final version of the paper.

Conflicts of interest: *The authors declare that there are no conflicts of interest associated with this manuscript.*

Financial support: *This work was supported by the National Natural Science Foundation of China, Nos. 61534003 (to ZGW) and 61874024 (to ZGW). The funding sources had no role in study conception and design, data analysis or interpretation, paper writing or deciding to submit this paper for publication.*

Institutional review board statement: *This study was approved by the Animal Research Committee of Southeast University, China (approval No. 20190720001) on July 20, 2019. The experimental procedure followed the United States National Institutes of Health Guide for the Care and Use of Laboratory Animals (NIH Publication No. 85-23, revised 1996).*

Data sharing statement: *Datasets analyzed during the current study are available from the corresponding author on reasonable request.*

Plagiarism check: *Checked twice by iThenticate.*

Peer review: *Externally peer reviewed.*

Open peer reviewer: *Ashraf S. Gorgey, Hunter Holmes Mcguire VA Medical Center, USA.*

Additional file: *Open peer review report 1.*

References

Angeli CA, Boakye M, Morton RA, Vogt J, Benton K, Chen Y, Ferreira CK, Harkema SJ (2018) Recovery of over-ground walking after chronic motor complete spinal cord injury. N Engl J Med 379:1244-1250.

Britten KH, Wezel RJAV (1998) Electrical microstimulation of cortical area MST biases heading perception in monkeys. Nat Neurosci 1:59-63.

Dalrymple AN, Everaert DG, Hu DS, Mushahwar VK (2018) A speed-adaptive intraspinal microstimulation controller to restore weight-bearing stepping in a spinal cord hemisection model. J Neural Eng 15:056023.

Fischer I, Dulin JN, Lane MA (2020) Transplanting neural progenitor cells to restore connectivity after spinal cord injury. Nat Rev Neurosci 21:366-383.

Formento E, Minassian K, Wagner F, Mignardot JB, Le Goff-Mignardot CG, Rowald A, Bloch J, Micera S, Capogrosso M, Courtine G (2018) Electrical spinal cord stimulation must preserve proprioception to enable locomotion in humans with spinal cord injury. Nat Neurosci 21:1728-1741.

Gad P, Choe J, Nandra MS, Zhong H, Roy RR, Tai YC, Edgerton VR (2013) Development of a multi-electrode array for spinal cord epidural stimulation to facilitate stepping and standing after a complete spinal cord injury in adult rats. J Neuroeng Rehabil 10:2.

GBD 2019 Viewpoint Collaborators (2020) Five insights from the Global Burden of Disease Study 2019. Lancet 396:1135-1159.

Gill ML, Grahn PJ, Calvert JS, Linde MB, Lavrov IA, Strommen JA, Beck LA, Sayenko DG, Van Straaten MG, Drubach DI, Veith DD, Thoreson AR, Lopez C, Gerasimenko YP, Edgerton VR, Lee KH, Zhao KD (2018) Neuromodulation of lumbosacral spinal networks enables independent stepping after complete paraplegia. Nat Med 24:1677-1682.

Gorgey AS, Black CD, Elder CP, Dudley GA (2009) Effects of electrical stimulation parameters on fatigue in skeletal muscle. J Orthop Sports Phys Ther 39:684-692.

Gorgey AS, Gill S, Holman ME, Davis JC, Atri R, Bai O, Goetz L, Lester DL, Trainer R, Lavis TD (2020) The feasibility of using exoskeletal-assisted walking with epidural stimulation: a case report study. Ann Clin Transl Neurol 7:259-265.

Gorgey AS, Mahoney E, Kendall T, Dudley GA (2006) Effects of neuromuscular electrical stimulation parameters on specific tension. Eur J Appl Physiol 97:737-744.

Grahn PJ, Mallory GW, Michael BB, Hachmann JT, Lobel DA, Luis LJ (2014) Restoration of motor function following spinal cord injury via optimal control of intraspinal microstimulation: toward a next generation closed-loop neural prosthesis. Front Neurosci 8:296.

Griffin JM, Bradke F (2020) Therapeutic repair for spinal cord injury: combinatory approaches to address a multifaceted problem. EMBO Mol Med 12:29.

Harkema S, Gerasimenko Y, Hodes J, Burdick J, Angeli C, Chen Y, Ferreira C, Willhite A, Rejc E, Grossman RG, Edgerton VR (2011) Effect of epidural stimulation of the lumbosacral spinal cord on voluntary movement, standing, and assisted stepping after motor complete paraplegia: a case study. Lancet 377:1938-1947.

Hofstoetter US, Danner SM, Freundl B, Binder H, Mayr W, Rattay F, Minassian K (2015) Periodic modulation of repetitively elicited monosynaptic reflexes of the human lumbosacral spinal cord. J Neurophysiol 114:400-410.

Holsheimer J (2002) Which neuronal elements are activated directly by spinal cord stimulation. Neuromodulation 5:25-31.

Huang ZH, Wang ZG, Lu XY, Li WY, Zhou YX, Shen XY, Zhao XT (2016) The principle of the micro-electronic neural bridge and a prototype system design. IEEE Trans Neural Syst Rehabil Eng 24:180-191.

Ichiyama RM, Yu PG, Zhong H, Roy RR, Edgerton VR (2005) Hindlimb stepping movements in complete spinal rats induced by epidural spinal cord stimulation. Neurosci Lett 383:339-344.

Jain NB, Ayers GD, Peterson EN, Harris MB, Morse L, O'Connor KC, Garshick E (2015) Traumatic Spinal Cord Injury in the United States, 1993-2012. JAMA 313:2236-2243.

Khanna VK (2016) Epidural spinal cord stimulation.in:implantable medical electronics: prosthetics, drug delivery, and health monitoring. Springer, Cham.

Ko HY, Ditunno JF, Graziani V, Little JW (1999) The pattern of reflex recovery during spinal shock. Spinal Cord 37:402-409.

Lavrov I, Courtine G, Dy CJ, van den Brand R, Fong AJ, Gerasimenko Y, Zhong H, Roy RR, Edgerton VR (2008) Facilitation of stepping with epidural stimulation in spinal rats: role of sensory input. J Neurosci 28:7774-7780.

Luo S, Xu H, Zuo Y, Liu X, All AH (2020) A review of functional electrical stimulation treatment in spinal cord injury. Neuromol Med 22:447-463.

Maynard FM, Bracken M, Creasey G, Ditunno JF, Donovan W, Ducker T, Garber S, Marino R, Stover S, Tator C, Waters R, Wilberger J, Young W (1997) International standards for neurological and functional classification of spinal cord injury. American Spinal Injury Association. Spinal Cord 35:266-274.

Minassian K, Jilge B, Rattay F, Pinter MM, Binder H, Gerstenbrand F, Dimitrijevic MR (2004) Stepping-like movements in humans with complete spinal cord injury induced by epidural stimulation of the lumbar cord: electromyographic study of compound muscle action potentials. Spinal Cord 42:401-416.

Murg M, Binder H, Dimitrijevic MR (2000) Epidural electric stimulation of posterior structures of the human lumbar spinal cord: 1. muscle twitches – a functional method to define the site of stimulation. Spinal Cord 38:394-402.

Nelson SG, Mendell LM (1978) Projection of single knee flexor Ia fibers to homonymous and heteronymous motoneurons. J Neurophysiol 41:778-787.

Nicolopoulos-Stournaras S, Iles JF (1983) Motor neuron columns in the lumbar spinal cord of the rat. J Comp Neurol 217:75-85.

Rahal M, Winter J, Taylor J, Donaldson N (2000) An improved configuration for the reduction of EMG in electrode cuff recordings: a theoretical approach. IEEE Trans Biomed Eng 47:1281-1284.

Rivero-Melián C (1996) Organization of hindlimb nerve projections to the rat spinal cord: a choleragenoid horseradish peroxidase study. J Comp Neurol 364:651-663.

Roy R, Hodgson J, Lauretz S, Pierotti D, Gayek R, Edgerton V (1992) Chronic spinal cord-injured cats: surgical procedures and management. Lab Anim Sci 42:335-343.

Shealy CN, Mortimer JT, Reswick JB (1967) Electrical inhibition of pain by stimulation of the dorsal columns: preliminary clinical report. Anesth Analg 46:489-491.

Shen X, Wang Z, Lv X, Huang Z (2013) Microelectronic neural bridging of toad nerves to restore leg function. Neural Regen Res 8:546-553.

Struijk JJ, Holsheimer J, Boom HBK (1993) Excitation of dorsal root fibers in spinal cord stimulation: a theoretical study. IEEE Trans Biomed Eng 40:632-639.

Tao C, Shen X, Ma L, Shen J, Li Z, Wang Z, Lu X (2019) Comparative study of intraspinal microstimulation and epidural spinal cord stimulation. Conf Proc IEEE Eng Med Biol Soc 2019:3795-3798.

Thier P, Andersen RA (1998) Electrical microstimulation distinguishes distinct saccade-related areas in the posterior parietal cortex. J Neurophysiol 80:1713-1735.

Wagner FB, Mignardot JB, Le Goff-Mignardot CG, Demesmaeker R, Komi S, Capogrosso M, Rowald A, Seáñez I, Caban M, Pirondini E, Vat M, McCracken LA, Heimgartner R, Fodor I, Watrin A, Seguin P, Paoles E, Van Den Keybus K, Eberle G, Schurch B, et al. (2018) Targeted neurotechnology restores walking in humans with spinal cord injury. Nature 563:65-71.

Wang H, Fang H, Dai J, Liu G, Xu ZJ (2013) Induced pluripotent stem cells for spinal cord injury therapy: current status and perspective. Neurol Sci 34:11-17.

Wang S, Zhang LC, Fu HT, Deng JH, Tang PF (2021) Epidural electrical stimulation effectively restores locomotion function in rats with complete spinal cord injury. Neural Regen Res 16:573-579.

Wang Z, Gu X, Lü X, Jiang Z, Li W, Lü G, Wang Y, Shen X, Zhao X, Wang H, Zhang Z, Shen H, Wu Y, Shen W, Zhang J, Chen D, Mao X, Shen H (2009) Microelectronics-embedded channel bridging and signal regeneration of injured spinal cords. Prog Nat Sci 19:1261-1269.

Wang ZG, Gu XS, Lu XY, Jiang ZL, Li WY, Lu GM, Wang YF, Wang HL, Zhang ZY, Shen HM, Yang W, Wei-Xing S, Jing-Yang Z, Dong C (2008) Microelectronic channel bridge and signal regeneration of injured spinal cords. conf Proc. of IEEE APCCAS 2008:658-661.

Wenger N, Moraud EM, Gandar J, Musienko P, Capogrosso M, Baud L, Le Goff CG, Barraud Q, Pavlova N, Dominici N, Minev IR, Asboth L, Hirsch A, Duis S, Kreider J, Mortera A, Haverbeck O, Kraus S, Schmitz F, DiGiovanna J, et al. (2016) Spatiotemporal neuromodulation therapies engaging muscle synergies improve motor control after spinal cord injury. Nat Med 22:138-145.

Wong SS, Chan CW, Cheung CW (2017) Spinal cord stimulation for chronic non-cancer pain: a review of current evidence and practice. Hong Kong Med J 23:517-523.

World Health Organization (2013) International perspectives on spinal cord injury. Weed Research 11:314-316.

Xu Q, Hu D, Duan B, He J (2015) A fully implantable stimulator with wireless power and data transmission for experimental investigation of epidural spinal cord stimulation. IEEE Trans Neural Syst Rehabil Eng 23:683-692.

Xu WL, Zuo Y, Xin DQ, He CY, Zhao P, Shi M, Zhou BY, Zhao YT, Zhao Y (2021) Selection of modeling methods for acute compressive spinal cord injury: a network Meta-analysis. Zhongguo Zuzhi Gongcheng Yanjiu 25:3767-3772.

Young AJ, Ferris DP (2017) State of the art and future directions for lower limb robotic exoskeletons. IEEE Trans Neural Syst Rehabil Eng 25:171-182.

Zheng Y, Mao YR, Yuan TF, Xu DS, Cheng LM (2020) Multimodal treatment for spinal cord injury: a sword of neuroregeneration upon neuromodulation. Neural Regen Res 15:1437-1450.

Zhou H, Xu Q, He J, Ren H, Zhou H, Zheng K (2012) A fully implanted programmable stimulator based on wireless communication for epidural spinal cord stimulation in rats. J Neurosci Methods 204:341-348.

P-Reviewer: Gorgey AS; C-Editor: Zhao M; S-Editors: Yu J, Wang J, Li CH; L-Editors: Brotchie A, Raye W, Qiu Y, Song LP; T-Editor: Jia Y